Simulating rare switching events of magnetic nanostructures with forward flux sampling

Christoph Vogler,* Florian Bruckner, Bernhard Bergmair, and Thomas Huber
Institute of Solid State Physics, Vienna University of Technology, Wiedner Hauptstrasse 8-10, 1040 Vienna, Austria

Dieter Suess
Christian Doppler Laboratory for Advanced Magnetic Sensing and Materials, Institute for Solid State Physics, Vienna University of Technology, Wiedner Hauptstrasse 8-10, 1040 Vienna, Austria

Christoph Dellago
University of Vienna, Faculty of Physics, Boltzmanngasse 5, 1090 Vienna, Austria
(Received 2 February 2013; revised manuscript received 14 August 2013; published 10 October 2013)

Predicting the thermal stability of magnetic storage devices is an important and challenging task. Here, we demonstrate how the forward flux sampling method (FFS) can be used to determine the thermal stability of magnets with general microstructures for time scales ranging from picoseconds to years. To apply FFS to magnetic systems, we first use the nudged elastic band (NEB) method to determine a minimum energy path connecting the initial with the final state of the magnetic transition. Interfaces defined based on this minimum energy path then provide the basis for the FFS procedure in which dynamical trajectories are generated by integrating a stochastic version of the fundamental equation of motion of the magnetization (Landau-Lifshitz-Gilbert equation) at finite temperature. This approach allows to determine average lifetimes for incoherent reversal processes and it can be applied for any value of the damping constant. We validate the method for a single-grain particle by comparison with the results of direct Langevin simulations carried out and demonstrate its capabilities and efficiency by computing the lifetime of a graded media grain, a magnetic structure with a tailored magnetocrystalline spatial anisotropy profile.

DOI: 10.1103/PhysRevB.88.134409 PACS number(s): 75.75.Jn, 75.78.Cd, 75.30.Kz, 75.50.Ss

I. INTRODUCTION

The prediction of the thermal stability of magnetic structures is important for numerous technological applications ranging from the design of magnetic recording structures and spin torque devices to the thermal decay of bulk permanent magnets.[1,2] A detailed knowledge of thermally activated reversal processes in magnetic structures is also crucial for the understanding of coercivity as function of temperature and sweep rates.[3] On a phenomenological level, thermal stability of magnetic states was successfully described using the Néel-Brown model. Within this framework, which relies on transition state theory, the rate constant k_{AB} quantifying the thermal stability of a magnetic state is calculated using the famous Arrhenius-Néel law

$$k_{AB} = \tau_0^{-1} e^{-\Delta E_{\mathrm{bar}}/k_{\mathrm{B}}T}, \tag{1}$$

where ΔE_{bar} denotes the lowest energy barrier separating the initial (meta)stable state from other long-lived states. The characteristic time τ_0 depends on the dynamics of the system and may be viewed as an attempt time related to the attempt frequency, $f_0 = \tau_0^{-1}$. Based on this expression, lifetimes of magnetic states were calculated for magnetic particles that reverse via coherent rotation both for overdamped dynamics[4,5] as well as in the small damping limit.[5–9] Ensembles of single-domain particles that are weakly coupled can be well described by Monte Carlo methods.[10]

While the thermally activated switching of single-domain particles has been studied exhaustively as documented in the literature,[11] there exists less work on the reversal of inhomogeneous magnetic structures. The thermal activation of domain walls was treated analytically for nanowires by Braun,[12] for soft/hard nanowires by Loxely *et al.*[13] and for nanowires with graded anisotropy by Visscher *et al.*[14] For more complicated structures, however, the activation energy cannot be computed analytically and one has to rely on numerical methods to determine the rate constant according to Eq. (1). Such a numerical computation can be performed in two steps. First, one determines the energy barrier ΔE_{bar} separating the long-lived states, for instance, using the nudged elastic band method (NEB) or the string method.[15–18] Then, one computes the prefactor f_0, a calculation that is numerically very challenging and has been performed only recently for arbitrary magnetic microstructures.[19]

Another strategy to calculate the thermal stability of magnetic nanostructures relies on the integration of the stochastic version of the Landau-Lifshitz-Gilbert equation. Such simulations, however, are restricted to several nanoseconds since small time steps are required to resolve the precessional motion.[20,21] Simulations of this type can be extended to longer times using temperature accelerated dynamics,[22,23] which exploits the larger rate constant at higher temperatures but reproduces the correct low-temperature behavior under the assumption that transition state theory holds. If this method is applied to the calculation of the switching rate of structures that are stable on the time scale of years, however, temperatures well above the Curie temperature are required to obtain the necessary acceleration. While such high temperatures pose no difficulty for single-domain particles, this approach fails for spin systems that are discretized in order to resolve domain walls. Also the bounce algorithm, in which the system is forced to stay in the high energy regions of configuration space, works best for single-domain particles.[24]

In this paper, we apply the forward flux sampling method,[25,26] originally developed for the simulation of rare events in biochemical networks, to the simulation of switching processes in magnetic microstructures. This method, which has been successfully applied to study a variety of rare events ranging from crystal nucleation to protein folding, is based on a staging procedure that selectively generates transition pathways without the necessity to simulate the system during the long waiting time between the transitions. In contrast to other path-based rare event simulation methods such as transition path sampling,[27–29] forward flux sampling does not require knowledge of the stationary phase space density, such that it can be easily applied to nonequilibrium systems. This feature makes the forward flux sampling methods also particularly suitable for the simulation of rare magnetic switching events in nonequilibrium situations, for instance, in the presence of time varying external fields. Here, we use this approach to determine lifetimes of advanced recording media, demonstrating that a small coercivity field can be combined with high thermal stability.

The remainder of the paper is organized as follows. In Sec. II, we introduce the equations of motion for the dynamics of micromagnetic structures driven by thermal fluctuations and briefly describe the forward flux sampling method for the calculation of rate constants. In Sec. III, a simple micromagnetic model is used to illustrate the calculation of the thermal stability of a magnetic particle by means of a combination of the nudged elastic band (NEB) method with forward flux sampling (FFS). The benefits concerning the computational cost of the presented FFS strategy in comparison to direct stochastic simulations are also discussed. In Sec. IV, the switching rate constant of a realistic graded media grain is computed and the transition path of the magnetization reversal is analyzed. Finally, the computational advantages of using the FFS method to determine average lifetimes of magnetic particles are summarized in Sec. V.

II. METHODS

A. Magnetization dynamics

The magnetization dynamics of a magnetic particle at finite temperature can be described with the stochastic version of the Landau-Lifshitz-Gilbert (LLG) equation,

$$\frac{d\hat{\boldsymbol{m}}}{dt} = -\frac{|\gamma|}{(1+\alpha^2)}\{\hat{\boldsymbol{m}} \times (\boldsymbol{H}_{\text{eff}} + \boldsymbol{H}_{\text{th}})\} - \frac{\alpha|\gamma|}{(1+\alpha^2)}\{\hat{\boldsymbol{m}} \times [\hat{\boldsymbol{m}} \times (\boldsymbol{H}_{\text{eff}} + \boldsymbol{H}_{\text{th}})]\}. \quad (2)$$

Here, $\hat{\boldsymbol{m}}$ is the magnetization of the magnetic particle normalized by the saturation magnetization M_S, γ is the reduced electron gyromagnetic ratio ($|\gamma| = |\gamma_e \mu_0| = 2.213 \times 10^5$ m/As), and α is the damping parameter. The effective magnetic field can be calculated as the functional derivative of the total energy with respect to the magnetization,

$$\boldsymbol{H}_{\text{eff}} = -\frac{1}{\mu_0 M_S}\frac{\delta E_{\text{tot}}}{\delta \hat{\boldsymbol{m}}}. \quad (3)$$

The thermal field $\boldsymbol{H}_{\text{th}}$ is an uncorrelated Gaussian random variable with zero mean and a variance following from the fluctuation-dissipation theorem,

$$\left\langle H_{\text{th},i}(t,\boldsymbol{r}) H_{\text{th},j}(t',\boldsymbol{r}')\right\rangle = 2D\delta_{ij}\delta(\boldsymbol{r}-\boldsymbol{r}')\delta(t-t'). \quad (4)$$

The total energy of the magnetic system is the sum of four contributions,

$$\begin{aligned} E_{\text{tot}} &= E_{\text{exc}} + E_{\text{ani}} + E_{\text{demag}} + E_{\text{Zee}} \\ &= \frac{\mathcal{J}S^2 c}{a}\int[(\nabla m_x)^2 + (\nabla m_y)^2 + (\nabla m_z)^2]dV \\ &\quad + \int K_1[1 - (\hat{\boldsymbol{e}}_{\text{easy}} \cdot \hat{\boldsymbol{m}})^2]dV \\ &\quad - \frac{\mu_0 M_S}{2}\int \hat{\boldsymbol{m}} \cdot \boldsymbol{H}_{\text{demag}} dV - \mu_0 M_S \int \hat{\boldsymbol{m}} \cdot \boldsymbol{H}_{\text{ext}} dV. \end{aligned} \quad (5)$$

The first term, E_{exc}, is the exchange energy, which arises from the exchange interactions between the magnetic moments. If only nearest-neighbor interactions are taken into account, the exchange integrals $\mathcal{J}$ can be assumed as constant. In this simplification, a is the lattice constant and $c = 1, 2$, and 4 for a simple cubic, bcc, and fcc lattice, respectively. The anisotropy energy E_{ani} originates from the crystal structure of the particle, which gives the magnetic moments a preferred direction. Such directions are called "easy directions" and are described by the unit vector $\hat{\boldsymbol{e}}_{\text{easy}}$. The constant K_1 in the second term is the anisotropy constant of the material. The third term, E_{demag}, represents the demagnetization energy, which arises because the demagnetization field $\boldsymbol{H}_{\text{demag}}$ of a magnetized structure tries to reduce its total magnetic moment by forming magnetic domains. The last term, the Zeeman energy E_{Zee}, comes from the interaction of the magnetic moments of the system with an external magnetic field $\boldsymbol{H}_{\text{ext}}$.

After rearranging Eq. (2), a system of Langevin equations with multiplicative noise results:[20,30]

$$\frac{d\hat{m}_i}{dt} = -A_i(\hat{\boldsymbol{m}},t) + B_{ik}(\hat{\boldsymbol{m}},t)\, H_{\text{th},k}(t). \quad (6)$$

The explicit expressions for $A_i(\hat{\boldsymbol{m}},t)$ and $B_{ik}(\hat{\boldsymbol{m}},t)$ are the same as in Ref. 30. Using a typical finite-element approach,[30] these equations can only be solved in the nanosecond time regime such that switching processes occurring on time scales of up to years are clearly out of reach of such simulations. However, while such switching events, which determine the thermal stability of magnetic systems, are rare, they proceed rapidly once they are initiated through a rare but important fluctuation. This fact is exploited in forward flux sampling, which concentrates on dynamical trajectories that include the switching event as described in the next section.

B. Forward flux sampling

The forward flux sampling (FFS) method[25] is a computational method for calculating rate constants of rare events, both in equilibrium and nonequilibrium systems. In this method, one considers rare transitions between long-lived states A and B, defined as regions in configuration space using an appropriate criterion. In between the states A and B, one then arranges a sequence of nonoverlapping interfaces defined as isosurfaces of an order parameter, $\lambda(x) = \lambda_i$, as illustrated schematically in Fig. 1. The value of the order parameter has to increase at

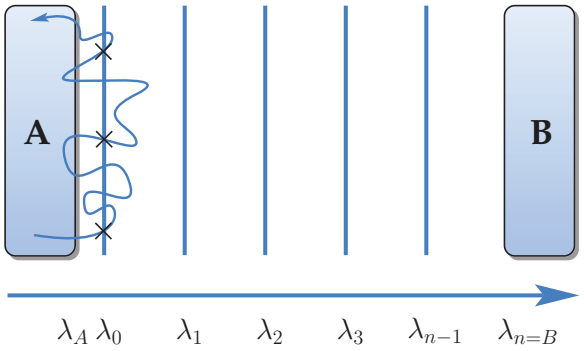

FIG. 1. (Color online) Schematic illustration of the stable states A and B and the interfaces λ_i that partition the configuration space between A and B into adjacent regions. In the first stage of a forward flux sampling simulation, one runs a trajectory starting in stable state A. Each time the trajectory exits region A and successively crosses interface λ_0, the system configuration is stored, as indicated by the crosses along λ_0.

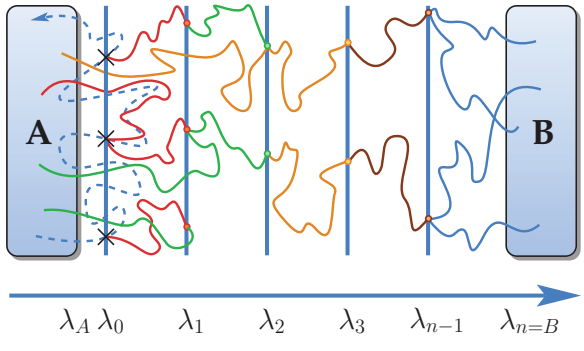

FIG. 2. (Color online) FFS algorithm: M_0 Langevin simulations are started from randomly chosen (previously stored) configurations at λ_0. Each simulation is terminated when the trajectory crosses the next interface, λ_1, or returns to A. This procedure is repeated at each interface until λ_n is reached.

each subsequent interface in comparison to the previous one, $\lambda_{i+1} > \lambda_i$. Furthermore, the interfaces need to be defined such that a trajectory evolving from A to B crosses each interface at least once. Multiple recrossings of an interface are allowed.

Based on this setup, the rate k_{AB} for transitions from A to B can be computed from the following expression:

$$k_{AB} = \Phi_{A,0} \prod_{i=0}^{n-1} P\left(\lambda_{i+1} \mid \lambda_i\right). \tag{7}$$

The first factor on the right-hand side of the equation, $\Phi_{A,0}$, is the rate at which trajectories coming from region A cross interface λ_0. The product following $\Phi_{A,0}$ is the probability that a trajectory crossing interface λ_0 reaches the final region B rather than returning to A first. Since this probability is small, it is written as a product of conditional probabilities that are easier to calculate. In Eq. (7), $P\left(\lambda_{i+1} \mid \lambda_i\right)$ denotes the probability that a trajectory that has crossed interface λ_i will cross interface λ_{i+1} before returning to A. The rate k_{AB} is the escape rate of the system for leaving the metastable state A and ending up in the metastable state B. The relaxation rate $k_R = k_{AB} + k_{BA}$ is the sum of the escape rate k_{AB} and the corresponding escape rate k_{BA} of the reversed transition from state B to state A. All examples in this work are symmetric in the sense that both escape rates are the same, because transitions from A to B and vice versa are equally probable. In this case, the relaxation rate k_R is simply twice the escape rate, $k_R = 2k_{AB}$. If the free energy of state A is not equal to the energy of state B, both escapes rates have to be determined with independent FFS simulations. In the FFS method, the factors appearing in Eq. (7) are computed as explained in the following.

First, a Langevin simulation is carried out in the stable state A (see Fig. 1). Each time the Langevin trajectory exits region A and successively crosses interface λ_0 the system configuration is stored. This initial simulation ends after a given number N_0 of crossings is stored. Then, one of these sampled configurations is selected at random and serves as starting point for a new Langevin simulation (see Fig. 2). This simulation is terminated after the system either reaches the next interface, λ_1, or returns to region A by crossing λ_A. If λ_1 has been reached, the system configuration at the crossing point is again stored. To collect a set of configurations at interface λ_1, this procedure is repeated M_0 times. From these configurations, new Langevin trajectories are started and propagated until they cross the next interface λ_2 or return to A (not just to the previous interface!). For the subsequent interfaces, one proceeds analogously. The whole procedure terminates successfully if at least one trajectory reaches the stable state B (crosses λ_n), or it terminates unsuccessfully if all trajectories coming from one of the interfaces return to A. In the first case, a rare switching event has occurred, in the second case, the choice of the interfaces has to be improved.

From the stored number of trajectories and the number of interface crossings, the rate constant of the rare switching event is calculated using Eq. (7). The first factor on the right-hand side of Eq. (7), $\Phi_{A,0}$, is estimated as the number of stored configurations at interface λ_0 divided by the total time of the Langevin simulation in region A. The transition probabilities $P\left(\lambda_{i+1} \mid \lambda_i\right)$ appearing in the product are computed as the number of trajectories that cross interface λ_{i+1} divided by the total number of trajectories started at interface λ_i. Multiplication of these factors finally yields the transition rate constant k_{AB}.

The most important and also the most challenging part of an FFS simulation is the suitable definition of the interfaces between the two stable states. If the interfaces are not chosen appropriately, no single trajectory will reach the final state B within the given simulation time and the FFS method will not yield any result. Here, we propose to place the interfaces along the minimum energy path of the magnetization reversal process obtained using the nudged elastic band (NEB) method,[15–17] as described in detail in Sec. III A. It has to be pointed out that the FFS algorithm is completely independent from the method used for placing the interfaces. Although the NEB method uses high damping to find energy minima and saddle points, the FFS method includes all dynamical effects of the system. The NEB method is just one, very efficient, way to arrange the interfaces between A and B. In principle, the results of forward flux sampling do not depend on the particular choice of the interfaces. However, not suitably chosen interfaces lead to a very poor efficiency of the method.

To quantify the accuracy of the FFS method, Allen *et al.* have derived analytical expressions for the statistical error affecting the transition rate constant.[31,32] To simplify the notation in the following, we define $p_i \equiv P(\lambda_{i+1} \mid \lambda_i)$ and $q_i \equiv 1 - p_i$ as well as $k_i \equiv M_i/N_0$ (ratio of the number of trial runs starting at interface λ_i and the number of configurations stored at λ_0). The relative variance of the transition rate constant is then given by

$$\mathcal{V} = \sum_{i=0}^{n-1} \frac{q_i}{p_i k_i} \left[\frac{1}{\prod_{j=0}^{i-1} \left(1 - q_j^{M_j}\right)} \right] \approx \sum_{i=0}^{n-1} \frac{q_i}{p_i k_i}. \qquad (8)$$

To determine $\mathcal{V}$, one assumes that the trajectories initiated at different interfaces are statistically independent from each other and that the variance of the transition rate constant originates only from the transition probabilities $P(\lambda_{i+1} \mid \lambda_i)$ rather than from the flux of trajectories out of the initial state A. This assumption usually holds for an appropriate definition of region A and sufficiently long simulation times. For a detailed derivation of Eq. (8), we refer the reader to Refs. 31 and 32. Borrero and Escobedo have demonstrated how to use the expression of Eq. (8) to optimize the efficiency of FFS-simulations either by a strategic placement of the interfaces or an asymmetric distribution of the computing effort on the interfaces.[33]

III. ILLUSTRATIVE MODEL

To demonstrate the application of the FFS approach to magnetic systems, we computed the average lifetime of a single-macrospin particle with dimensions of 1 nm × 1 nm × 1 nm, which is described with one single spin. The particle has an anisotropy constant of $K_1 = 3\ \mathrm{MJ/m^3}$, a saturation polarization of $\mu_0 M_S = 0.5$ T and its easy axis is pointing in the z direction. In addition, a homogeneous external magnetic field is applied along the negative y direction, which we will call the perpendicular external field in the following. The magnetic dynamics of such a particle is fully specified by the vector magnetization $\hat{\boldsymbol{m}}(t)$ on the surface of the unit sphere in three dimensions as a function of time t. Different field strengths are used and the temperature of the Langevin simulation is adapted to get a constant exponent of the Arrhenius-Néel law $\Delta E_{\mathrm{bar}} = 9 k_B T$ for each field strength. There are three reasons for using this simple superparamagnetic single-spin model. (1) For the parameters considered here, the magnetization reversal process can be monitored in one single direct Langevin simulation of length 10^4 ns. In this case, it is possible to count the number of switches directly and from this number the thermal stability of the system (quantified by the average lifetime) can be computed. The results obtained in this way provide the basis to test the FFS approach. (2) Kalmykov gives an analytical formula[4] to compute the thermal stability of single-macrospin particles under the influence of arbitrary homogeneous magnetic fields, which offers another possibility of comparison. (3) The model is very instructive because the magnetic configurations of such a particle can be visualized as normalized vectors moving on the unit sphere. Such a visualization is not possible with analogous hypervectors of a full micromagnetic model.

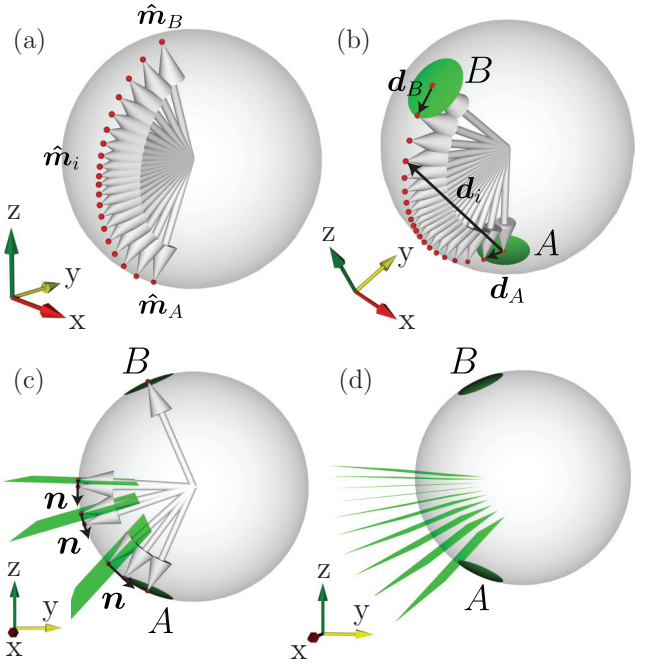

FIG. 3. (Color online) FFS interface definition for the single-macrospin model with a perpendicular external magnetic field applied in the negative y direction. (a) Minimum energy path of magnetization reversal from $\hat{\boldsymbol{m}}_A$ to $\hat{\boldsymbol{m}}_B$. (b) Euclidean norm definition of the stable states A and B. (c) Definition of the interfaces λ_0 to λ_{n-1} with hyperplanes. (d) Final hybrid interface definition.

A. Interface definition

In the first step of the FFS procedure, the minimum energy path of the magnetization reversal is determined. Since our goal is to simulate a reversal from the magnetization-down to the magnetization-up state, the NEB calculation is carried out for start and end configurations with magnetizations in the $-z$ and $+z$ directions, respectively. The NEB procedure then yields the minimum energy configurations [$\hat{\boldsymbol{m}}_A$ and $\hat{\boldsymbol{m}}_B$ in Fig. 3(a)] as well as intermediate configurations along the minimum energy path [$\hat{\boldsymbol{m}}_i$ in Fig. 3(a)]. Note that the magnetization in the energy minima is not pointing in the z direction because of the perpendicular external applied magnetic field in the $-y$ direction.

In the next step, the interfaces λ_A and λ_B of the stable states A and B around the energy minima need to be properly defined. We define A and B by requiring that the deviation of the magnetization from the magnetization of the respective minimum energy configuration is smaller than a given value,

$$|\hat{\boldsymbol{m}} - \hat{\boldsymbol{m}}_{A,B}| < \lambda_{A,B}, \qquad (9)$$

where the vertical bars denote the Euclidean norm. It is important to choose the stable states A and B sufficiently narrow. Otherwise it may happen that a magnetization trajectory, which is only precessing around $\hat{\boldsymbol{m}}_B$ with a small opening angle, but which indeed returns to $\hat{\boldsymbol{m}}_A$ afterwards, is counted as a magnetic reversal trajectory (because it crossed the border interface λ_B). Such trajectories are known as "U turns". In case of superparamagnetic particles, they are frequently occurring error sources. If they are not correctly recognized, the rate constants are clearly overestimated. To obtain the correct rate

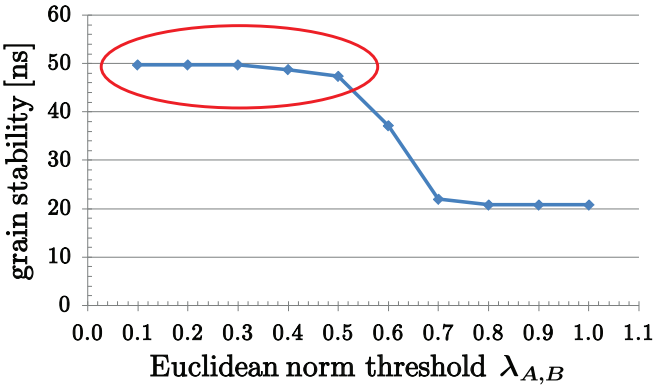

FIG. 4. (Color online) Grain stability of the illustrative model plotted against the Euclidean norm threshold $\lambda_{A,B}$ used to define the stable states A and B. A perpendicular external magnetic field with strength of 40% of the anisotropy field is applied. In the marked area, the evaluated grain stability is independent of the threshold value. Thus it represents the "real" stability, which is not affected by "U turns."

constant, it has to be ensured that k_{AB} is independent from the chosen value of $\lambda_{A,B}$, for decreasing Euclidean norm threshold. This means that the rate constant should not change if the energy minimum definition is made even stricter. Simulations with too large $\lambda_{A,B}$ result in an overestimation of the rate constant, because "U turns" are counted as magnetization reversals. This behavior is demonstrated in Fig. 4 for the illustrative model with a perpendicular external applied field with a strength of 40% of the anisotropy field. It follows for all presented calculations, the definitions of the stable states A and B, and thus the criteria for magnetization reversals, are suitable to guarantee that the system stays in a minimum, if its magnetization falls below $\lambda_{A,B}$, until a new rare event takes place. This holds for arbitrary damping of the system.

For the interfaces 0 to $n-1$, a different definition is used. As shown in Fig. 3(c), first, the vector to the previous magnetic configuration along the minimum energy path is calculated,

$$\boldsymbol{n}_i = \hat{\boldsymbol{m}}_i - \hat{\boldsymbol{m}}_{i-1}. \tag{10}$$

Interface i is then defined as the plane (or hyperplane if a full micromagnetic model is used) that passes through $\hat{\boldsymbol{m}}_i$ and is normal to $\boldsymbol{n}_i$. Note that in the string method, the interfaces are also defined as hyperplanes normal to the string.[16] To decide whether an interface has been crossed, the position of the current magnetization $\hat{\boldsymbol{m}}(t)$ vector relative to the hyperplane has to be determined. This can be done by computing the scalar product

$$\boldsymbol{n}_i \cdot [\hat{\boldsymbol{m}}(t) - \hat{\boldsymbol{m}}_i] \tag{11}$$

and checking its sign at each time step. The final interface definition is shown in Fig. 3(d). In summary, stable states A and B are defined with the Euclidean distance to the minimum energy configurations. In between, hyperplanes are arranged along the minimum energy path. Note that there are only planes from region A up to the transition state of the magnetization reversal transition, because the probability of a trajectory starting from a hyperplane near the transition state to reach region B is sufficiently high. As a consequence, additional interfaces are not necessary and would only add to the computational cost without improving the accuracy of the calculation. With this interface definition the FFS method can be applied as described in the next section.

B. Results

As mentioned in Sec. III, we select the temperature such that the energy barrier $\Delta E_{\text{bar}} = 9k_{\text{B}}T$, which is sufficiently small to observe several magnetization reversals in a single direct Langevin simulation of length 10^4 ns. To detect a switch between the stable states, the magnetization trajectory is followed on the surface of the unit sphere. The stable magnetic states are defined with the same Euclidean norm approach as used in the FFS approach (see Sec. III A) and a threshold value of 0.5 for the distance from the energy minima is taken. In the FFS method, the stable states A and B are defined by the requirement that the Euclidean distance from the energy minima is less than 0.45. With these definitions the resulting rate constants are independent from the Euclidean norm threshold in both methods, as shown in Fig. 4. The rate constants thus arise purely from "real" magnetization reversals, which means that switched trajectories stay in their energy minima until a new rare switching event occurs. For both simulation methods, a damping parameter of $\alpha = 0.02$ is used.

Thermal stabilities (quantified by average lifetimes) obtained from the direct simulations for perpendicular external fields of 0%–40% of the anisotropy field are shown in Fig. 5 as dashed blue line. For each field strength, five Langevin simulations of 10^4 ns were carried out. The red solid line in Fig. 5 is the thermal stability calculated with the FFS method. Mean values of five simulations and the corresponding standard deviations are plotted. An optimization of the interface positions was performed for each field strength, such that the flux of partial trajectories through all interfaces is nearly constant.[33]

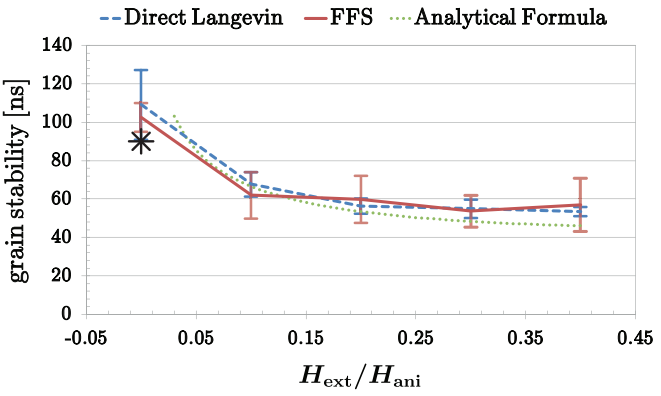

FIG. 5. (Color online) Thermal grain stability quantified by the average lifetime of the magnetic state for perpendicular homogeneous external magnetic fields with different field strengths. The FFS results (red solid line) and the direct Langevin simulation results (blue dashed line) are averages over five simulations. All simulations were performed with a damping constant of $\alpha = 0.02$. The error bars indicate the standard deviation of the attempt frequency (σ_{S}) based on repeated simulations with a certainty interval of 68.3%. The analytical behavior derived in Ref. 4 for the considered single-macrospin particle is shown as green dotted line. The analytically calculated value at zero field, according to Ref. 34, is shown by a black star.

TABLE I. FFS simulation results for perpendicular external fields with a strength of 0%–40% of the anisotropy field. The crossing probabilities $\bar{p}_0$ to $\bar{p}_3$, the average lifetime $\bar{\tau}$, the prefactor (attempt frequency) $\bar{f}_0$, and the relative variance $\bar{\mathcal{V}}$ of $\bar{f}_0$ are average values over five separate simulations. σ_S is the standard deviation of $\bar{f}_0$ based on repeated FFS simulations and $\sigma_\mathcal{V}$ is estimated from the relative variance of the prefactor according to Eq. (12).

$\frac{H_{ext}}{H_{ani}}$	$\bar{p}_0$	$\bar{p}_1$	$\bar{p}_2$	$\bar{p}_3$	$\bar{\tau}$ (ns)	$\bar{f}_0$ (GHz)	$\bar{\mathcal{V}}$	$\sigma_\mathcal{V}$ (GHz)	σ_S (GHz)
0.0	0.27	0.29	0.30	0.31	102.43	80.26	0.51	5.75	10.70
0.1	0.33	0.30	0.33	0.33	62.04	132.50	0.44	8.80	17.72
0.2	0.34	0.38	0.32	0.33	59.98	140.21	0.41	8.98	31.66
0.3	0.31	0.31	0.28	0.32	53.80	156.28	0.48	10.80	31.81
0.4	0.29	0.33	0.30	0.32	56.99	144.05	0.47	9.84	17.96

The results of these simulations are listed in Table I. The crossing probabilities $\bar{p}_i$, average lifetimes $\bar{\tau}$, prefactors (attempt frequencies) $\bar{f}_0$, and the relative variances $\bar{\mathcal{V}}$ of $\bar{f}_0$ shown in the table are averages over five independent FFS simulations. The statistical error of the prefactor, $\sigma_\mathcal{V}$, is estimated from the relative variance $\mathcal{V}$ of the transition rate constant,

$$\sigma_\mathcal{V} = \sqrt{\frac{\mathcal{V} f_0^2}{N_0}}, \tag{12}$$

where N_0 is the number of stored configurations at interface λ_0. If the simulation results of the direct Langevin and the FFS simulations are compared, it can be seen that the two methods yield results that are identical up to the statistical errors. The green dotted line shows the thermal stability predicted by transition state theory (TST) as derived analytically by Kalmykov[4] for single-macrospin particles. In the case of perpendicular external fields, the TST prediction is only valid for $H_{ext} \geqslant 0.04 H_{ani}$. Figure 5 shows that the simulation results are also in a good agreement with Kamlmykov's analytical expression. At zero field, there exists an analytical expression of Brown,[34] which also agrees with the prediction of the FFS method within its statistical error limit (see Fig. 5).

In the following, we compare the computational effort required by the FFS method and by direct Langevin simulations to determine thermal stabilities of the discussed single-spin model. In all simulations, a damping parameter of $\alpha = 0.02$ is used and a perpendicular external magnetic field with strength of 10% of the anisotropy field is applied. In direct Langevin simulations, a sufficient number of spontaneous switches of the magnetization has to be collected in order to ensure statistically significant results. Therefore the computational cost of direct Langevin simulations increases exponentially with increasing energy barrier as indicated in Fig. 6. Thus direct Langevin simulations for the calculation of thermal stabilities are only effective if the energetic barrier is not much larger than the thermal energy $k_B T$. The FFS approach, however, is not affected by this restriction, but can deal with arbitrarily high energetic barriers and, therefore, with very large lifetimes of magnetic states.

Table II shows the parameters and the results of the FFS simulations for different energy barriers. For each barrier $\Delta E_{bar}/k_B T$, five independent FFS simulations were performed. Figure 7 illustrates that the FFS results again agree well with the analytical formula of Ref. 4. The dependence of the required CPU hours with respect to the energy barrier (see Fig. 6) can be explained as follows. For increasing energy barrier, additional interfaces have to be inserted between the two stable states A and B to ensure that the crossing probabilities from one interface to the next remain approximately constant. The single Langevin trajectories used to compute the crossing probabilities have almost the same length for all energy barriers, they even get a bit shorter for increasing barrier heights, because the relaxation of the magnetization in the two energy minima is faster. As a consequence, the total simulation time increases almost linearly with the number of interfaces. An additional increase in CPU time is due to the larger number of trajectories generated at each interface (higher k_i) needed to keep the relative statistical variance $\mathcal{V}$ constant (if p_i remains constant). The results shown in Fig. 6 imply that the total simulation times required by the two methods are only comparable for the simple illustrative model discussed in Sec. III B. For a magnetic grain with a more realistic energy barrier, it is not possible to determine the thermal stability with direct Langevin simulations, but with the FFS approach a calculation with good accuracy can be performed in about 55 CPU hours. One point which should be mentioned is that in Tables I and II, the standard deviations of the repeated simulations σ_S are significantly larger than the corresponding standard deviations $\sigma_\mathcal{V}$, which can be calculated from a single

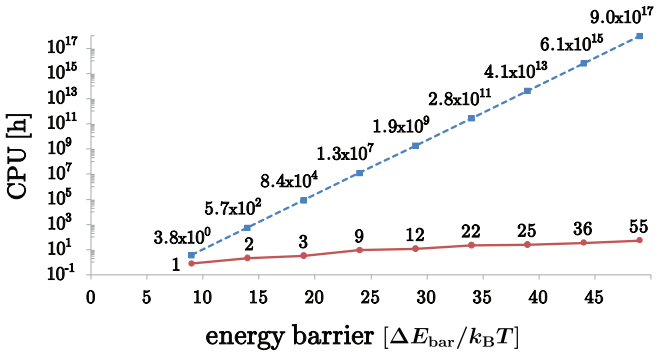

FIG. 6. (Color online) Total simulation times on a single-core machine for single-macrospin particles with different energy barriers (the exact CPU times are shown in the data labels). The simulation parameters are the same as those used to obtain the results shown in Fig. 5. For the direct simulation, the required CPU time increases exponentially with increasing energy barrier ΔE_{bar} (blue dashed line extrapolated from simulation with $\Delta E_{bar} = 9 k_B T$). For the FFS method, the total simulation time increases linearly with the number of interfaces and the number of trajectories per interface (red solid line).

TABLE II. Computational setup (number of interfaces $n_{\text{interfaces}}$, range of average crossing probabilities $\bar{p}_i$) and results of FFS simulations (attempt frequency $\bar{f}_0$, relative variance $\mathcal{V}$, standard deviations σ_S, $\sigma_\mathcal{V}$, and total simulation times in CPU hours) for different energy barriers $\Delta E_{\text{bar}}/k_B T$ of the illustrative model of Sec. III. A perpendicular external magnetic field with strength of 10% of the anisotropy field is applied. These are the FFS results of Fig. 6 in detail. Quantities with an overbar denote average values of five independent FFS simulations.

$\Delta E_{\text{bar}}/k_B T$	$n_{\text{interfaces}}$	$\bar{p}_i$ (min–max)	$\bar{f}_0$ (GHz)	$\sigma_\mathcal{V}$ (GHz)	σ_S (GHz)	CPU (h)
9	4	0.30–0.33	132.50	8.80	17.72	1
14	7	0.24–0.33	152.43	10.57	40.01	2
19	10	0.23–0.27	171.29	15.08	32.25	3
24	13	0.19–0.29	228.36	16.70	46.13	9
29	16	0.18–0.29	278.26	23.08	77.10	12
34	19	0.21–0.26	288.75	21.48	121.69	22
39	22	0.20–0.27	310.62	25.52	131.27	25
44	25	0.16–0.28	403.41	35.35	112.41	36
49	27	0.17–0.25	305.89	25.40	121.15	55

FFS simulation according to Eqs. (8) and (12). A small mismatch can be explained by the fact that $\sigma_\mathcal{V}$ just accounts for statistical errors in the transition probabilities $P(\lambda_{i+1} \mid \lambda_i)$ between the FFS interfaces. The prefactor $\Phi_{A,0}$ in Eq. (7) is supposed to be exact, which is not completely true in our simulations. There are still small deviations of $\Phi_{A,0}$ between the repeated simulations. But these deviations are too small to explain the gap between σ_S and $\sigma_\mathcal{V}$. To reveal the true nature of this discrepancy, further investigations have to be performed.

IV. GRADED MEDIA GRAIN

To reveal the full power of the FFS method, we have used it to simulate the thermal reversal process of a full micromagnetic graded media grain. The grain model is a 20-nm-long prism with a pentagonal basal plane (outer radius of 2.1 nm) studied at a temperature of 300 K. As given in Ref. 35, the minimum switching field is obtained for a quadratic increase of the anisotropy profile. According to Ref. 35,

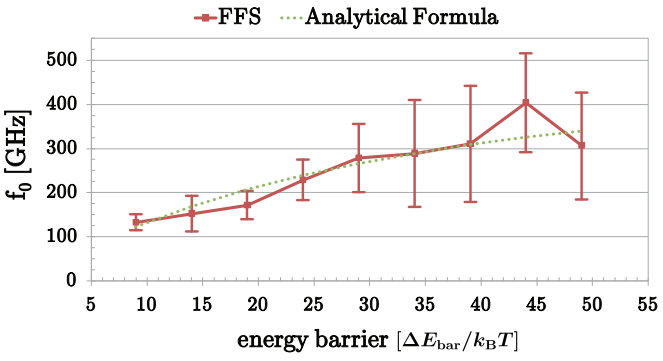

FIG. 7. (Color online) Attempt frequencies [prefactors of Eq. (1)] of the illustrative single-macrospin model for different energy barriers $\Delta E_{\text{bar}}/k_B T$. A perpendicular external magnetic field with strength of 10% of the anisotropy field is applied. The FFS results (red solid line) are averages of five independent simulations and the error bars show the standard deviations σ_S of these repetitions (68.3% certainty). All detailed results can be found in Table II. The analytically derived values according to Ref. 4 (green dotted line) agree well with the FFS results. For better visualization, the attempt frequency instead of the grain stability is shown in this plot, because the grain stability varies over several magnitudes due to the different energy barriers.

the grain is partitioned into eight different materials with such a quadratically increasing anisotropy profile $K_1(z) = z^2 1.24 \times 10^{22}$ J/m^5 [see Fig. 8(a)]. The magnetic polarization $\mu_0 M_S = 0.5$ T and the exchange constant $A = 10^{-11}$ J/m are the same in all parts of the grain. A finite element mesh size of 2 nm and a damping parameter of $\alpha = 0.02$ are used for the micromagnetic simulations. The spatial discretization of the model consists of 62 nodes, 167 volume elements, and 125 surface elements. Since the grain has a uniaxial anisotropy pointing along the z axis, we compute the attempt frequency of the thermal magnetization reversal from a magnetization-down to a magnetization-up state. After calculating the minimal energy path of the rotation with the NEB method, 29 interfaces (λ_0 to $\lambda_{n=28}$) between the two stable states A (magnetization-down) and B (magnetization-up) are defined for the FFS algorithm. The positions of the interfaces are optimized, according to the procedure described in Ref. 33, such that the flux of partial trajectories through the interfaces is almost constant ($15\% \leqslant p_i \leqslant 22\%$).

Selected configurations along one of the transition paths obtained from the FFS simulation, which required a total of 12 600 CPU hours, are shown in Fig. 8. The beginning of the magnetization reversal can be seen in Fig. 8(a), which displays a magnetic configuration observed at the first interface, λ_0. In the lower, magnetically soft part of the grain, the magnetic moments start to precess around the easy axis. As the reversal process goes on, the rotating moments move upwards on the grain and a domain wall forms, which is clearly developed at interface λ_6 as shown in Fig. 8(b). Figures 8(c) and 8(d) show the domain wall moving from the magnetically softer parts of the grain to the magnetically harder parts. Finally, the system reaches the last interface λ_B [a configuration from this interface is shown in Fig. 8(e)] and the magnetization reversal is completed. Combining the flux out of region A with the crossing probabilities for all interfaces yields a thermal stability of $\tau = 1417$ years. With the energy barrier $\Delta E_{\text{bar}} = 53.32\, k_B T_{300}$ determined in the NEB method, this thermal stability corresponds to the attempt frequency $f_0 = 3215.21$ GHz according to Eq. (1). The relative statistical variance of the attempt frequency obtained using Eq. (8) is $\mathcal{V} = 0.28$, yielding a standard deviation of $\sigma_\mathcal{V} = 212.67$ GHz according to Eq. (12). If a certainty interval of 3 $\sigma_\mathcal{V}$ (99.7% certainty) is used, the average particle lifetime is at least

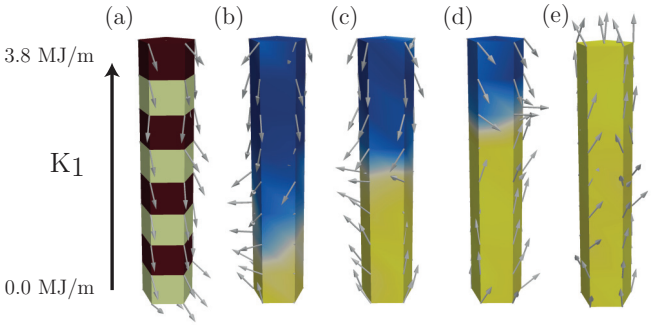

FIG. 8. (Color online) Magnetic configurations along a thermal magnetization reversal path of a graded media grain with quadratically increasing anisotropy. The basal plane of the model is a pentagon with an outer radius of 2.1 nm. (a) The color code shows the eight different materials of the grain and the magnetization vectors show a magnetic configuration at interface λ_0. (b)–(e) Magnetic configurations at interfaces λ_6 (b), λ_{16} (c), λ_{25} (d), and λ_B (e). The color code illustrates the z component of the total normalized magnetization.

1135 years. This is obviously a thermally stable grain, although the presented particle has a significantly smaller diameter than grains of single phase recording media. The variance and thus the standard deviation of the transition rate can be decreased if the number of trial runs started at each interface is increased while the number of configurations stored at interface λ_0 remains constant (k_i increases), or if additional interfaces are inserted (p_i increases). Since trajectories started at different interfaces should be uncorrelated to optimize efficiency, k_i should be increased first.

V. CONCLUSION

In conclusion, we have demonstrated that the thermal stability of magnetic particles can be predicted accurately and efficiently with the forward flux sampling method. To apply FFS, we have divided the configuration space between the two stable magnetic states using interfaces defined as hyperplanes normal to the minimum energy path of the magnetization reversal. The resulting thermal stabilities are in good agreement with direct Langevin simulations of single-macrospin particles with a low-energy barrier. The total simulation time for calculating the thermal stability of magnetic particles, however, is significantly lower if the FFS method is used. To illustrate the potential of FFS, we simulated the magnetization reversal of a graded media grain with realistic dimensions. Our results validate the concept of graded media, which combines a reduced coercivity with a thermal stability still sufficiently large even for diameters much smaller than those of single phase recording grains.

ACKNOWLEDGMENTS

Financial support of the Austrian Science Fund FWF, Project SFB-ViCoM, F4112-N13, of the Vienna Science and Technology Fund WWTF, Project MA09-029, and of the Austrian Federal Ministry of Economy, Family and Youth and the National Foundation for Research, Technology and Development, are gratefully acknowledged.

*christoph.vogler@tuwien.ac.at

[1] T. Kawahara, K. Ito, R. Takemura, and H. Ohno, Microelectron. Reliab. **52**, 613 (2012).
[2] G. Hrkac, T. G. Woodcock, C. Freeman, A. Goncharov, J. Dean, T. Schrefl, and O. Gutfleisch, Appl. Phys. Lett. **97**, 232511 (2010).
[3] D. Suess, L. Breth, J. Lee, M. Fuger, C. Vogler, F. Bruckner, B. Bergmair, T. Huber, J. Fidler, and T. Schrefl, Phys. Rev. B **84**, 224421 (2011).
[4] Y. P. Kalmykov, J. Appl. Phys. **96**, 1138 (2004).
[5] W. T. Coffey, D. S. F. Crothers, J. L. Dormann, L. J. Geoghegan, and E. C. Kennedy, Phys. Rev. B **58**, 3249 (1998).
[6] V. I. Mel'nikov and S. V. Meshkov, J. Chem. Phys. **85**, 1018 (1986).
[7] P. M. Déjardin, D. S. F. Crothers, W. T. Coffey, and D. J. McCarthy, Phys. Rev. E **63**, 021102 (2001).
[8] D. A. Garanin, E. C. Kennedy, D. S. F. Crothers, and W. T. Coffey, Phys. Rev. E **60**, 6499 (1999).
[9] L. J. Geoghegan, W. T. Coffey, and B. Mulligan, Adv. Chem. Phys. **100**, 475 (1997).
[10] R. W. Chantrell, N. Walmsley, J. Gore, and M. Maylin, Phys. Rev. B **63**, 024410 (2000).
[11] W. T. Coffey and Y. P. Kalmykov, J. Appl. Phys. **112**, 121301 (2012).
[12] H. B. Braun, J. Appl. Phys. **76**, 6310 (1994).
[13] P. N. Loxley and R. L. Stamps, Phys. Rev. B **73**, 024420 (2006).
[14] P. Visscher and R. Zhu, Physica B **407**, 1340 (2012).
[15] G. Henkelman, B. P. Uberuaga, and H. Jónsson, J. Chem. Phys. **113**, 9901 (2000).
[16] Weinan E, Weiqing Ren, and Eric Vanden-Eijnden, Phys. Rev. B **66**, 052301 (2002).
[17] R. Dittrich, T. Schrefl, D. Suess, W. Scholz, H. Forster, and J. Fidler, J. Magn. Magn. Mater. **250**, 12 (2002).
[18] E. Paz, F. Garcia-Sanchez and O. Chubykalo-Fesenko, Physica B **403**, 330 (2008).
[19] G. Fiedler, J. Fidler, J. Lee, T. Schrefl, R. L. Stamps. H. B. Braun and D. Suess, J. Appl. Phys. **111**, 093917 (2012).
[20] J. L. García-Palacios and F. J. Lázaro, Phys. Rev. B **58**, 14937 (1998).
[21] E. Boerner and H. Bertram, IEEE T. Magn. **33**, 3052 (1997).
[22] A. F. Voter, Phys. Rev. Lett. **78**, 3908 (1997).
[23] J. Xue and R. H. Victora, Appl. Phys. Lett. **77**, 3432 (2000).
[24] S. Wang and P. B. Visscher, IEEE T. Magn. **43**, 2893 (2007).
[25] R. J. Allen, P. B. Warren and P. R. ten Wolde, Phys. Rev. Lett. **94**, 018104 (2005).
[26] R. J. Allen, D. Frenkel and P. R. ten Wolde, J. Chem. Phys. **124**, 024102 (2006).

[27]C. Dellago, P. G. Bolhuis, F. S. Csajka, and D. Chandler, J. Chem. Phys. **108**, 1964 (1998).
[28]P. G. Bolhuis, D. Chandler, C. Dellago, and P. L. Geissler, Annu. Rev. Phys. Chem. **53**, 291 (2002).
[29]T. S. van Erp, D. Moroni, and P. G. Bolhuis, J. Chem. Phys. **118**, 7762 (2003).
[30]W. Scholz, T. Schrefl, and J. Fidler, J. Magn. Magn. Mater. **233**, 296 (2001).
[31]R. J. Allen, D. Frenkel and P. R. ten Wolde, J. Chem. Phys. **124**, 194111 (2006).
[32]R. J. Allen, C. Valeriani and P. Rein ten Wolde, J. Phys.-Condens. Mat. **21**, 463102 (2009).
[33]E. E. Borrero and F. A. Escobedo, J. Chem. Phys. **129**, 024115 (2008).
[34]W. F. Brown, Phys. Rev. **130**, 1677 (1963).
[35]D. Suess, J. Fidler, G. Zimanyi, T. Schrefl, and P. Visscher, Appl. Phys. Lett. **92**, 173111 (2008).